Robust Medical X-Ray Image Classification by Deep Learning with Multi-Versus Optimizer

Thirugnanam Kumar

Department of Computer and Information Science, Annamalai University, India
kumarddeau@gmail.com (corresponding author)

Ramasamy Ponnusamy

Department of Computer and Information Science, Annamalai University, India
povi2006@gmail.com

ABSTRACT

Classification of medical images plays an indispensable role in medical treatment and training tasks. Much effort and time are required in the extraction and selection of classification features of medical images. Deep Neural Networks (DNNs) are an evolving Machine Learning (ML) method that has proved its ability in various classification tasks. Convolutional Neural Networks (CNNs) present the optimal results for changing image classification tasks. In this regard, this study focused on developing a Multi-versus Optimizer with Deep Learning Enabled Robust Medical X-ray Image Classification (MVODL-RMXIC) method, aiming to identify abnormalities in medical X-ray images. The MVODL-RMXIC model used the Cross Bilateral Filtering (CBF) technique for noise removal, a MixNet feature extractor with an MVO algorithm based on hyperparameter optimization, and Bidirectional Long-Short-Term Memory (BiLSTM) for image classification. The proposed MVODL-RMXIC model was simulated and evaluated, showing its efficiency over other current methods.

Keywords-medical X-ray images; biomedical imaging; image classification; deep learning; multi-versus optimizer

I. INTRODUCTION

Automated systems to detect abnormalities in medical X-ray images have become a challenge in the ML domain [1]. The expansive anatomical varieties for individual patients are one of the most severe problems in radiograph projection with superimposed frameworks [2]. Radiologists apply practical knowledge and their skills to analyze X-ray images and detect fractures in bones [3]. The quality of medical images captured with image capture tools is often poor. Therefore, it is challenging for physicians to identify abnormalities, and a potentially automated Computer Aided Detection (CAD) mechanism was devised in [4] to overcome this issue. Therefore, automated recognition of abnormalities in X-ray images can be helpful for physicians in identifying numerous clinical problems such as osteoporosis, arthritis, bone cancer, infection fracture, and dental decay [5].

Researchers in Artificial Intelligence (AI) make a large contribution to data processing [6]. Advances in AI can transform healthcare by considering medical treatments and diagnostics as data problems. Deep Learning (DL) is a subdivision of ML that extracts detailed features from data and has been proven to be very effective in many data processing tasks [7]. DL is becoming an eminent solution for a wide range of text processing or Natural Language Processing (NLP),

speech recognition and synthesis, Computer Vision (CV) tasks, and signal analysis [8]. CNN, a multi-layered Neural Network (NN), is essential in several digital image processing tasks such as segmentation, object recognition, pattern detection, classification, and feature extraction in many kinds of images, including healthcare images [9]. DL needs a plethora of data to achieve suitable results and is resource-hungry. Transfer Learning (TL), which is an ML method, has been proposed to solve this problem. TL repurposes a technique trained on a single task on a second relevant task. To achieve maximum accuracy, pre-trained approaches were re-trained on small data with fewer trainable variables [10]. Based on the selected method and data, pre-trained methods were optimally tuned to attain promising results.

This study developed the Multi-Versus Optimizer with Deep Learning enabled Robust Medical X-Ray Image Classification (MVODL-RMXIC) method, using the Cross Bilateral Filtering (CBF) approach for noise removal, a MixNet feature extractor with an MVO algorithm based on hyperparameter optimization, and the Bidirectional Long Short-Term Memory (BiLSTM) method for image classification. A far-reaching simulation process was carried out to evaluate the effectiveness of the proposed MVODL-RMXIC method.

II. RELATED WORKS

In [11], a Chest X-Ray (CXR) imaging categorization method of COVID-19 artifacts under altered real-time conditions was presented, using a new CNN based on Bayesian optimization. This method used CNN to extract and learn deep features and Bayesian-based optimization to tune CNN hyperparameters based on the primary function. In [12], a FractalCov-Net infrastructure was established using Fractal blocks and U-Net to segment chest CT images to detect areas of lesion. A similar FractalCov-Net setting was also used to classify CXR images using TL. Different approaches were used, such as FCN, U-Net, Segnet, DenseU-Net, and ResnetU-Net. Classification results were compared with different algorithms, namely VGG16, ResNet5, Xception, DenseNet, and InceptionResNetV2 structures. In [13], CXR imaging was used to detect COVID-19 and pneumonia in a 3-stage process. The main stage involved segmented raw X-ray imaging using a conditional generative adversarial network. In the second phase, pulmonary image segmentation was performed as a novel pipeline, integrating key point extraction approaches and a DNN trained to extract discrimination factors. In [14], state-of-the-art techniques were used to classify X-ray images of potential tuberculosis patients. A vital improvement was observed if coarse-to-fine data transfer can be used to fine-tune the method using several data augmentation systems.

In [15], a novel method was presented to detect COVID-19, using a C-GAN to generate synthetic images to increase the restricted count of accessible data, presenting two DL techniques. This study focused on either a binary classifier for COVID-19 vs a normal case or a multiclassifier that contains a tertiary class for bacterial pneumonia. In [16], an ML system was introduced to recognize COVID-19 in CXR images. The features extracted by HOG and CNN in X-ray images were fused for classification with a VGGNet CNN. The MADF system can be used to optimally preserve edges and decrease noise from the image. A watershed segmenting system can be used to mark a critical fracture part from the input X-ray image.

III. THE PROPOSED MODEL

This paper presents the MVODL-RMXIC method to detect and classify medical X-ray images. The proposed model aimed to identify abnormalities in medical X-ray images, encompassing CBF noise removal, MixNet feature extraction, MVO-based tuning process, and LSTM-based classification. Figure 1 illustrates the block model of MVODL-RMXIC.

A. Stage I: Image Filtering Process

CBF was used for noise removal, as it can decide the range distancing through the captured guide image in diverse photographic circumstances instead of the target image [17]. This method may alleviate quality loss whenever the image is too noisy and has pseudo- or unsharp edging. The theoretical variances among the original and cross-BF appear to be insignificant. BF plays a significant role in smoothing tasks by appropriately substituting guides and target images. Consider the BF enforced on a 2D grayscale image x. Let $q \in \mathcal{N}_p$ denote a neighboring pixel of p, where $p \in Z^2$ signify the location of the target pixel, $\mathcal{N}_p \subset Z^2$ is the neighboring pixel set at p, which is a rectangle domain assisted in a filter window,

and $x_p \in \mathbb{R}^1$ designates its pixel intensity. Using such notation, BF can be given as follows:

$$BF(p) := \frac{\sum_{q \in N_p} w_S(p,q) \cdot w_r(g_p, g_q) \cdot x_q}{\sum_{q \in N_p} w_S(p,q) \cdot w_r(g_p, g_q)} \tag{1}$$

where g_q is one of its neighboring pixels, and g_p is a target pixel in the guide image. This definition was equal to the novel BF if it is self-guided, i.e., $g_p = x_p$ and $g_q = x_q$.
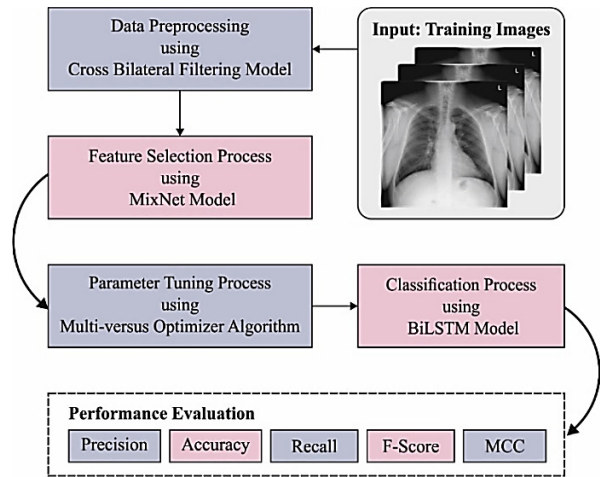

Fig. 1.   Block diagram of the MVODL-RMXIC model

B. Stage II: Feature Extraction Process

In this phase, the MVODL-RMXIC method used a MixNet feature extractor, as shown in Figure 2.
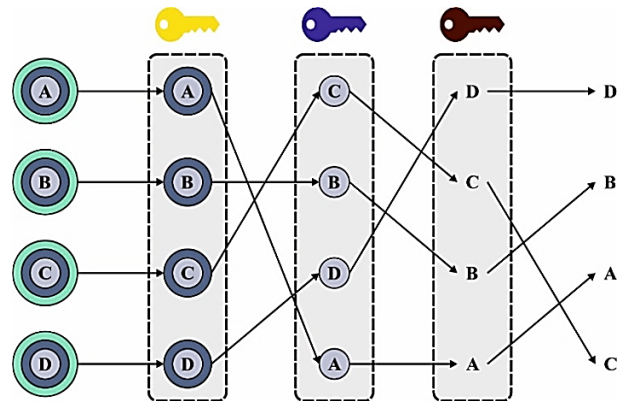

Fig. 2.   Structure of the MixNet model.

Mixed Depthwise Conv (MixConv) Kernels would extend vanilla depthwise convolution through several kernel sizes in a single Conv [18]. MixConv merges several kernel sizes in one Conv by dividing the input of Conv into groups and implementing diverse kernel sizes in all groups. Unlike vanilla depthwise Conv, MixConv can capture various paradigms from Conv input at several resolutions. Similarly, it needs some parameters and is more computationally effective than employing one kernel. For example, using several kernels [(3, 3),(5, 5),(7, 7)] is more computationally effective than using a

7×7 single kernel. Then, it uses various kernels for all groups, and finally, the three results are linked to generate the last complex result. Figure 2 presents the structure of MixNet.

Then, the MVO algorithm was used, which is based on hyperparameter optimization [19]. MVO is a populace-based technique stimulated by the big-bang theory. The proposed method performed the search process using two stages: (i) exploration and (ii) exploitation. The concept of black holes and white holes was used to explore the search space, and the wormhole concept was used to introduce the exploiting stage. In multiverse theories, a black hole attracts everything. A wormhole connects different places in the universe and plays the role of interconnecting tunnels among diverse universes. Every universe has its inflation rate. The MVO attributes every resolution with an inflating rate corresponding to the fitness function. According to MVO, the subsequent rules are used in optimization:

- A high rate of inflation in the universe is making it have additional white holes, and, on the other hand, the probability of consisting black holes dropping.

- Contrary to a universe with a smaller inflation rate, a universe with a huge inflation rate is prone to dispatching objects to others via a white hole. In contrast, the universe with the lowest inflating rate tends to obtain objects through black holes.

- Despite the rate of inflation, the object transmits arbitrarily toward a better universe through a wormhole.

In MVO, the object (search agent) moves among diverse universes via white or black holes. A roulette wheel approach is applied for mathematical modeling, and the black/white hole tunnel transmits the procedure of objects among universes. Initially, many universes are constructed to create a multiverse. Next, using the iterative method, the universe is sorted according to its inflation rate. Then, the universe is carefully chosen to possess a white hole through the roulette wheel.

The optimizing procedure begins by producing various universes. In the optimization method, two variables dictate solution changes and can be evaluated to update the solution: (i) Traveling Distance Rates (TDRs) and (ii) Wormhole Existence Probability (WEP).

$$WEP = a + t \times \left(\frac{b-a}{T}\right) \tag{2}$$

$$TDR = 1 - \frac{t^{1/p}}{T^{1/p}} \tag{3}$$

where a and b are the minimum and maximum numbers ($a = 0.2$ and $b = 1$), and T and t indicate the maximum and the existing iteration amounts, respectively. Consider that there are n candidate solutions and d variables that are the number of universes. After defining WEP and TDR variables, the position of the solution was upgraded according to the following:

$$i_{i(i=1,2,...,n)}^{j(j=1,2,...,d)} =$$
$$\begin{cases} \begin{cases} X_j + TDR \times \left((ub_j - lb_j) \times r_4 + lb_j\right); r_3 < 0.5 \\ X_j - TDR \times \left((ub_j - lb_j) \times r_4 + lb_j\right); r_3 > 0.5 \end{cases} & r_2 < WEP \\ x_i^j & r_2 \geq WEP \end{cases} \tag{4}$$

where x_i^j specifies the j-th parameters of the i-th universe, X_j denotes the j-th variable of the better universe, lb_j and ub_j denote the low and high limiting of the j-th variables correspondingly, and r_2, r_3, and r_4 indicate three random number ranges within [0, 1].

C. Stage III: X-Ray Image Classification Process

The BiLSTM method was used for image classification. LSTM proposed a particular memory cell for temporal dataset storage. This architecture allows recalling long-range features more than conventional RNNs [20]. Through multi-layer models, the cell component at the i-th time step at the l layer in the forward direction is carried out by the following:

$$f_i^l = \sigma\left(W_{(f)}^l \vec{h}_i^{l-1} + V_{(f)}^l \vec{h}_{i-1}^l + b_{(f)}^l\right) \tag{5}$$

$$i_i^l = \sigma\left(W_{(i)}^l \vec{h}_i^{l-1} + V_{(i)}^l \vec{h}_{i-1}^l + b_{(i)}^l\right) \tag{6}$$

$$0_i^l = \sigma\left(W_{(0)}^l \vec{h}_i^{l-1} + V_{(0)}^l \vec{h}_{i-1}^l + b_{(0)}^l\right) \tag{7}$$

$$g_i^l = \tanh\left(W_{(g)}^l \vec{h}_i^{l-1} + V_{(g)}^l \vec{h}_{i-1}^l + b_{(g)}^l\right) \tag{8}$$

$$C_i^l = f_i^l \odot C_{i-1}^l + i_i^l \odot g_i^l \tag{9}$$

$$\vec{h}_i^l = 0_i^l \odot \tanh\left(C_i^l\right) \tag{10}$$

In these expressions, f_i^l refers to forget gate, i_i^l denotes the input gate, 0_i^l signifies the output gate, g_i^l implies the hidden state, and C_i^l is a candidate gate. σ and hyperbolic tangent functions were used as activating functions, W^l denotes the weighted matrix among layer cells $(l-1) - l$, $\vec{h}_i^l$ indicates the sigmoid function, V^l signifies the weight matrix amongst sequential l layer cells, b^l denotes the bias vector in the total layers, $\odot$ represents component-wise multiplication, and N^l the dimension vector magnitude. The sequence length distributes the bias value and weight matrix in a cell, thereby reducing the comprehensive amount of weights and hidden neurons in the network. A BLSTM will process the data in the backward and forward directions with two different LSTM layers. The $\vec{h}_i^l$, forward HL is computed through the above-mentioned formula, and the back-state, $\overleftarrow{h}_i^l$ is concatenated and then fed into the subsequent layer:

$$\vec{h}_i^l = \begin{bmatrix} \vec{h}_i^l, \\ \overleftarrow{h}_i^l \end{bmatrix} \tag{11}$$

where $l = 0$ indicates the input layer. BLSTM is good at achieving the correlations among components in a whole sequence through information instead of recalling the features in one direction. Furthermore, using the variable sharing model, BLSTM needs less memory to resolve problems compared to the FNN and CNN mechanisms.

IV. PERFORMANCE VALIDATION

The proposed MVODL-RMXIC method was simulated using Python 3.6.5 on an i5-8600K, 16GB RAM, GeForce 1050Ti 4GB, 250GB SSD, and 1TB HDD PC, with the following parameters: dropout: 0.5, batch size: 5, epoch count: 50, learning rate: 0.01, and activation function: ReLU. The COVID-19 radiography dataset [21] was used to evaluate the

method, which has images in three categories: Normal, COVID, and Viral Pneumonia (VP). Figure 3 shows some sample images and Figure 4 shows the confusion matrix of the MVODL-RMXIC method on the X-Ray image classification process.
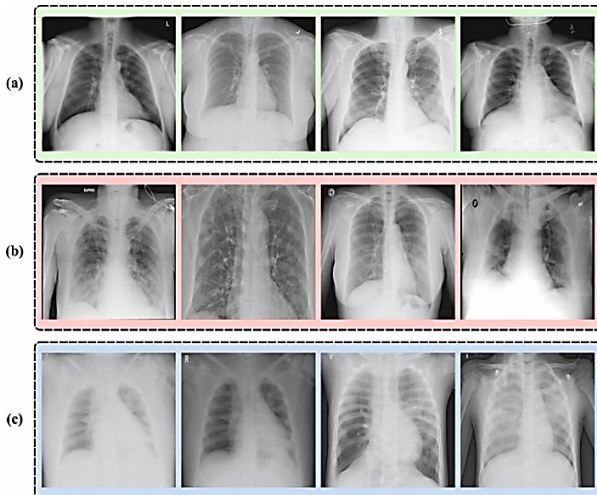
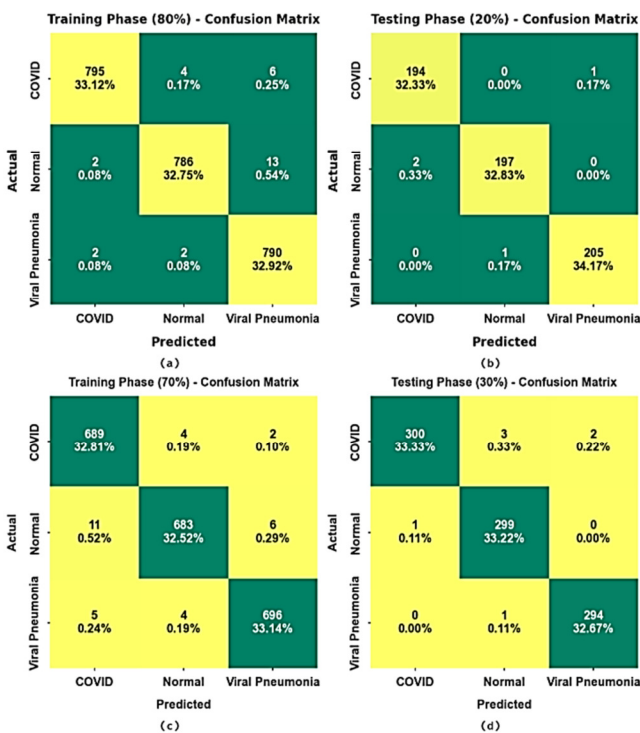

Fig. 3.   (a) COVID, (b) normal, and (c) VP.

Fig. 4.   Confusion matrix of the MVODL-RMXIC method (a-b) 80:20 TR/TS, and (c-d) 70:30 TR/TS.

The output of the MVODL-RMXIC method was effective in all classes. Table I shows the classification results of the MVODL-RMXIC method in an 80:20 proportion for TR and TS of the dataset. Figures 5 and 6 show the classification results of the MVODL-RMXIC method on the 80% TR and the

20% TS of the dataset, respectively, demonstrating its efficiency in all cases. In the COVID class, the MVODL-RMXIC model obtained an increased $accu_y$ of 99.42% and 99.50%, $prec_n$ of 99.50% and 98.98%, $reca_l$ of 98.76% and 99.49%, F_{score} of 99.13%, and 99.23% and MCC of 98.69% and 98.86%, for 80% TR and 20% TS of the dataset, respectively.

TABLE I.   OUTPUT ANALYSIS OF MVODL-RMXIC UNDER 80:20 TR:TS DATA

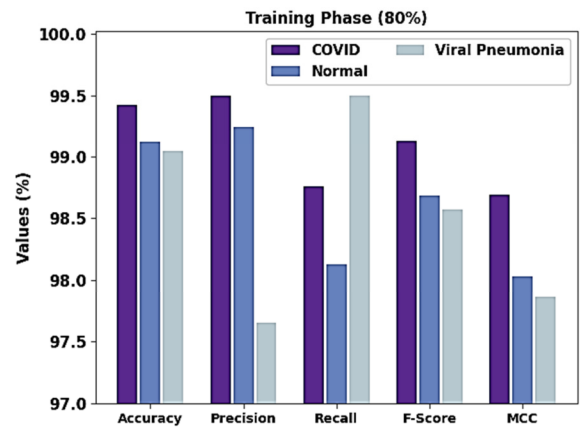| Labels	$accu_y$	$prec_n$	$reca_l$	F_{score}	MCC
Training (80%)					
COVID	99.42	99.50	98.76	99.13	98.69
Normal	99.12	99.24	98.13	98.68	98.03
VP	99.04	97.65	99.50	98.57	97.86
Average	**99.19**	**98.80**	**98.79**	**98.79**	**98.19**
Testing (20%)					
COVID	99.50	98.98	99.49	99.23	98.86
Normal	99.50	99.49	98.99	99.24	98.87
VP	99.67	99.51	99.51	99.51	99.26
Average	**99.56**	**99.33**	**99.33**	**99.33**	**99.00**

Fig. 5.   Evaluation of MVODL-RMXIC system under 80% TR dataset.
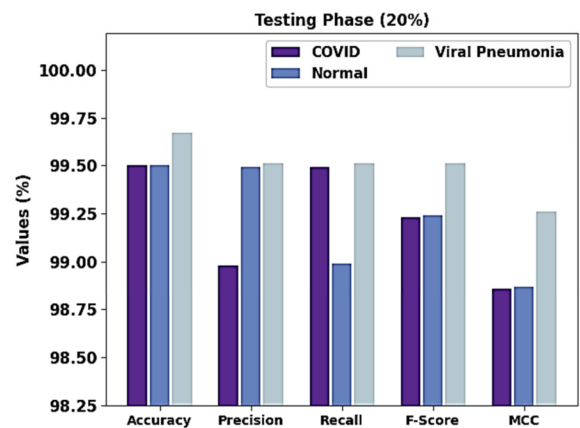

Fig. 6.   Evaluation of MVODL-RMXIC method in 20% TS dataset.

Table II shows the classification results of MVODL-RMXIC in a 70:30 TR/TS proportion of the dataset, demonstrating its efficiency in all cases. In the COVID class, the MVODL-RMXIC method had $accu_y$ of 98.95%, $prec_n$ of

97.73%, $reca_l$ of 99.14%, F_{score} of 99.43%, and MCC of 97.65%. Similarly, in standard class, the MVODL-RMXIC approach attained an increased $accu_y$ of 98.81%, $prec_n$ of 98.84%, $reca_l$ of 97.57%, F_{score} of 98.20%, and MCC of 97.32%. In the VP class, the MVODL-RMXIC method achieved an increased $accu_y$ of 99.19%, $prec_n$ of 98.86%, $reca_l$ of 98.72%, F_{score} of 98.79%, and MCC of 98.18%. Table III shows a comparison of MVODL-RMXIC with other methods [22, 23]. The results show that the SqueezeNet and VGG19 models showed the least $accu_y$ values of 92.96% and 93.30%, respectively, followed by the TL_SqueezeNet and ResNet-1with 96.44% and 97.23%, respectively. In contrast, the TL_ResNet-2 method showed a considerable $accu_y$ of 98.44% but the MVODL-RMXIC model reached a higher $accu_y$ of 99.56%.

TABLE II.   EVALUATION OF MVODL-RMXIC MODEL UNDER 70:30 TR:TS OF THE DATASET

Labels	$accu_y$	$prec_n$	$reca_l$	F_{score}	MCC
Training (70%)					
COVID	98.95	97.73	99.14	98.43	97.65
Normal	98.81	98.84	97.57	98.20	97.32
VP	99.19	98.86	98.72	98.79	98.18
Average	**98.98**	**98.48**	**98.48**	**98.47**	**97.72**
Testing (30%)					
COVID	99.33	99.67	98.36	99.01	98.51
Normal	99.44	98.68	99.67	99.17	98.76
VP	99.67	99.32	99.66	99.49	99.24
Average	**99.48**	**99.22**	**99.23**	**99.22**	**98.84**

TABLE III.   RELATIVE EVALUATION OF MVODL-RMXIC WITH OTHER METHODS

Models	$accu_y$	$prec_n$	$reca_l$
SqueezeNet	92.96	91.73	95.10
TL_SqueezeNet	96.44	96.08	96.84
VGG_19	93.30	91.78	94.73
TL_ResNet2	98.44	97.97	97.94
ResNet1	97.23	96.74	97.43
MVODL-RMXIC	99.56	99.33	99.33

V.   CONCLUSION

This study developed a novel MVODL-RMXIC method for detecting and classifying medical X-ray images, aiming to identify abnormalities. The proposed MVODL-RMXIC method used the CBF technique for noise removal, a MixNet feature extractor with an MVO algorithm based on hyperparameter optimization, and the BiLSTM model for image classification. A wide-ranging simulation analysis was carried out, showing the effectiveness of MVODL-RMXIC and its improved performance over other current methods. In future work, hybrid DL classifiers could be integrated to boost the performance of the MVODL-RMXIC method.

REFERENCES

[1] J. I. Z. Chen, "Design of Accurate Classification of COVID-19 Disease in X-Ray Images Using Deep Learning Approach," *Journal of IoT in Social, Mobile, Analytics, and Cloud*, vol. 3, no. 2, pp. 132–148, Jun. 2021.

[2] S. Chakraborty, S. Paul, and K. M. A. Hasan, "A Transfer Learning-Based Approach with Deep CNN for COVID-19- and Pneumonia-Affected Chest X-ray Image Classification," *SN Computer Science*, vol.

3, no. 1, Oct. 2021, Art. no. 17, https://doi.org/10.1007/s42979-021-00881-5.

[3] U. Subramaniam, M. M. Subashini, D. Almakhles, A. Karthick, and S. Manoharan, "An Expert System for COVID-19 Infection Tracking in Lungs Using Image Processing and Deep Learning Techniques," *BioMed Research International*, vol. 2021, Nov. 2021, Art. no. e1896762, https://doi.org/10.1155/2021/1896762.

[4] R. Kumar et al., "Accurate Prediction of COVID-19 using Chest X-Ray Images through Deep Feature Learning model with SMOTE and Machine Learning Classifier." 2020, https://doi.org/10.1101/2020.04.13.20063461.

[5] A. A. Reshi et al., "An Efficient CNN Model for COVID-19 Disease Detection Based on X-Ray Image Classification," *Complexity*, vol. 2021, May 2021, Art. no. e6621607, https://doi.org/10.1155/2021/6621607.

[6] P. K. Mall and P. K. Singh, "BoostNet: a method to enhance the performance of deep learning model on musculoskeletal radiographs X-ray images," *International Journal of System Assurance Engineering and Management*, vol. 13, no. 1, pp. 658–672, Mar. 2022, https://doi.org/10.1007/s13198-021-01580-3.

[7] K. KC, Z. Yin, M. Wu, and Z. Wu, "Evaluation of deep learning-based approaches for COVID-19 classification based on chest X-ray images," *Signal, Image and Video Processing*, vol. 15, no. 5, pp. 959–966, Jul. 2021, https://doi.org/10.1007/s11760-020-01820-2.

[8] H. Munusamy, K. J. Muthukumar, S. Gnanaprakasam, T. R. Shanmugakani, and A. Sekar, "FractalCovNet architecture for COVID-19 Chest X-ray image Classification and CT-scan image Segmentation," *Biocybernetics and Biomedical Engineering*, vol. 41, no. 3, pp. 1025–1038, Jul. 2021, https://doi.org/10.1016/j.bbe.2021.06.011.

[9] R. Kumar et al., "Classification of COVID-19 from chest x-ray images using deep features and correlation coefficient," *Multimedia Tools and Applications*, vol. 81, no. 19, pp. 27631–27655, Aug. 2022, https://doi.org/10.1007/s11042-022-12500-3.

[10] I. D. Apostolopoulos and T. A. Mpesiana, "Covid-19: automatic detection from X-ray images utilizing transfer learning with convolutional neural networks," *Physical and Engineering Sciences in Medicine*, vol. 43, no. 2, pp. 635–640, Jun. 2020, https://doi.org/10.1007/s13246-020-00865-4.

[11] T. Akhtar, N. G. Haider, and S. M. Khan, "A Comparative Study of the Application of Glowworm Swarm Optimization Algorithm with other Nature-Inspired Algorithms in the Network Load Balancing Problem," *Engineering, Technology & Applied Science Research*, vol. 12, no. 4, pp. 8777–8784, Aug. 2022, https://doi.org/10.48084/etasr.4999.

[12] T. N. Le, H. M. V. Nguyen, T. A. Nguyen, T. T. Phung, and B. D. Phan, "Optimization of Load Ranking and Load Shedding in a Power System Using the Improved AHP Algorithm," *Engineering, Technology & Applied Science Research*, vol. 12, no. 3, pp. 8512–8519, Jun. 2022, https://doi.org/10.48084/etasr.4862.

[13] M. Bhalekar and M. Bedekar, "D-CNN: A New model for Generating Image Captions with Text Extraction Using Deep Learning for Visually Challenged Individuals," *Engineering, Technology & Applied Science Research*, vol. 12, no. 2, pp. 8366–8373, Apr. 2022, https://doi.org/10.48084/etasr.4772.

[14] O. Yadav, K. Passi, and C. K. Jain, "Using Deep Learning to Classify X-ray Images of Potential Tuberculosis Patients," in *2018 IEEE International Conference on Bioinformatics and Biomedicine (BIBM)*, Madrid, Spain, Sep. 2018, pp. 2368–2375, https://doi.org/10.1109/BIBM.2018.8621525.

[15] S. Karakanis and G. Leontidis, "Lightweight deep learning models for detecting COVID-19 from chest X-ray images," *Computers in Biology and Medicine*, vol. 130, Mar. 2021, Art. no. 104181, https://doi.org/10.1016/j.compbiomed.2020.104181.

[16] N.-A.- Alam, M. Ahsan, M. A. Based, J. Haider, and M. Kowalski, "COVID-19 Detection from Chest X-ray Images Using Feature Fusion and Deep Learning," *Sensors*, vol. 21, no. 4, Jan. 2021, Art. no. 1480, https://doi.org/10.3390/s21041480.

[17] K. Shirai, K. Sugimoto, and S. Kamata, "Adjoint Bilateral Filter and Its Application to Optimization-based Image Processing," *APSIPA Transactions on Signal and Information Processing*, vol. 11, no. 1, Apr. 2022, https://doi.org/10.1561/116.00000046.

[18] J. Ou and H. Wu, "Efficient Human Pose Estimation with Depthwise Separable Convolution and Person Centroid Guided Joint Grouping," in *Pattern Recognition and Computer Vision*, Nanjing, China, 2020, pp. 626–638, https://doi.org/10.1007/978-3-030-60639-8_52.

[19] R. M. A. Ikram, H. L. Dai, A. A. Ewees, J. Shiri, O. Kisi, and M. Zounemat-Kermani, "Application of improved version of multi verse optimizer algorithm for modeling solar radiation," *Energy Reports*, vol. 8, pp. 12063–12080, Nov. 2022, https://doi.org/10.1016/j.egyr. 2022.09.015.

[20] X. Liu, S. Liu, X. Li, B. Zhang, C. Yue, and S. Y. Liang, "Intelligent tool wear monitoring based on parallel residual and stacked bidirectional long short-term memory network," *Journal of Manufacturing Systems*, vol. 60, pp. 608–619, Jul. 2021, https://doi.org/10.1016/ j.jmsy.2021.06.006.

[21] "COVID-19 Radiography Database." https://www.kaggle.com/datasets/ tawsifurrahman/covid19-radiography-database.

[22] S. H. Khan, A. Sohail, A. Khan, and Y.-S. Lee, "COVID-19 Detection in Chest X-ray Images Using a New Channel Boosted CNN," *Diagnostics*, vol. 12, no. 2, Feb. 2022, Art. no. 267, https://doi.org/10.3390/diagnostics12020267.

[23] M. Ragab, S. Alshehri, N. A. Alhakamy, W. Alsaggaf, H. A. Alhadrami, and J. Alyami, "Machine Learning with Quantum Seagull Optimization Model for COVID-19 Chest X-Ray Image Classification," *Journal of Healthcare Engineering*, vol. 2022, Mar. 2022, Art. no. e6074538, https://doi.org/10.1155/2022/6074538.